Synthesis and characterization of silk ionomers for layer-by-layer electrostatic deposition on individual mammalian cells

Onur Hasturk, Jugal Kishore Sahoo, David L. Kaplan*

Department of Biomedical Engineering, Tufts University, 4 Colby Street, Medford, MA 02155, USA

*Corresponding author

E-mail address: david.kaplan@tufts.edu

Abstract

Nanocoating of individual mammalian cells with polymer layers has been of increasing interest in biotechnology and biomedical engineering applications. Electrostatic layer-by-layer (LbL) deposition of polyelectrolytes on negatively charged cell surfaces has been utilized for cell nanocoatings using synthetic or natural polymers with a net charge at physiological conditions. Here, our previous synthesis of silk-based ionomers through modification of silk fibroin (SF) with polyglutamate (PG) and polylysine (PL) was exploited for the nanocoating of mammalian cells. SF-PL constructs were cytotoxic to mammalian cells, thus an alternative approach for the synthesis of silk ionomers through carboxylation and amination of regenerated SF chains was utilized. Through the optimization of material properties and composition of incubation buffers, silk ionomers could be electrostatically assembled on the surface of murine fibroblasts and human mesenchymal stem cells (hMSCs) to form nanoscale multilayers without significantly impairing cell viability. The resulting silk-based protein nanoshells were transient and degraded over time, allowing for cell proliferation. The strategies presented here provide a basis for the cytocompatible nanoencapsulation of mammalian cells within silk-based artificial cell walls, with potential

benefits for future studies on surface engineering of mammalian cells, as well as for utility in cell therapies, 3D printing and preservation.

Keywords: silk ionomers, mammalian cells, nanocoating, nanoencapsulation, layer-by-layer assembly

Introduction

Unlike prokaryotes, unicellular eukaryotes or fungi, animal cells are enclosed only by a fluidic, fragile plasma membrane and do not have cell walls or exoskeletal shells to protect them against harsh environmental conditions. Nanoencapsulation of individual mammalian cells in thin and tough polymer shells has been proposed as a potential strategy to form artificial cell walls for protection against physical and chemical stresses and immune attacks applied during *ex vivo* and *in vivo* manipulation such as tissue engineering applications and cell therapy. [1, 2] Several approaches including binding of biopolymers to surface receptors [3-8], matrix-ion complexation [9, 10], and *in situ* polymerization or crosslinking on cell surface [11-14] have been demonstrated for the encapsulation of individual mammalian cells. The most common strategy, however, has been the electrostatic layer-by-layer (LbL) assembly of polyelectrolytes or minerals, [2, 15-25] which is widely employed for the formation of nanoscale multilayer films on charged surfaces [26-28] or nanoencapsulation of bacteria, yeast [29-33] or pancreatic islands. [34-36] The net negative charge of plasma membrane allows for electrostatic aggregation of positively charged polyelectrolytes onto cell surface, enabling deposition of a negatively charged polyelectrolyte as the second layer. By alternating incubation in aqueous solutions of oppositely charged substrates, it is possible to assemble nanoscale multilayers on cell surfaces and the composition and thickness can easily be tuned by altering the type and number of the layers deposited. [2, 37]

Despite the large variety of cytocompatible polyanions such as poly(styrene sulfonate) (PSS), polyacrylic acid (PAA), hyaluronic acid (HA) and alginate, the number of polycations suitable for deposition on living mammalian cells is limited due to potential cytotoxicity through damaging the integrity of plasma membrane. [17, 38, 39] For example, PL, a polycation that is widely used for surface coatings to enhance cell adhesion to substrates, [40] could be lethal to mammalian cells in suspension even at low concentrations since it may form nanoscale holes in plasma membrane and induce necrotic death. [38, 41] Many studies on nanoencapsulation of mammalian cells have been limited with the use of gelatin [17, 23, 24], which is an amphoteric polyelectrolyte containing both positively (arginine, lysine) and negatively charged amino acids (glutamate, aspartate) and therefore displays limited electrostatic affinity to negatively charged substrates. [42] Although some solved this issue by using cationized gelatin and demonstrated nanocoating of live cancer cells [19, 25], others documented potential cytotoxicity of cationized gelatin on healthy cells such as human osteoblasts [43] or murine fibroblasts. [44] In a recent study, cytotoxicity of the polycation layer was avoided through the formation of a negatively charged framing template on the cells by insertion of cholesterol-DNA conjugates into the plasma membrane followed by supramolecular complexation of alginate-DNA conjugates. [45] However, insertion of anchor molecules in plasma membrane may have unpredicted impacts such as alterations in membrane fluidity, inactivation of membrane-bound enzymes or ion transporters [46] or elevated production of reactive oxygen species. [47] Therefore, it is essential to develop cytocompatible polycations that can be safely deposited on cell surface with minimum effect on viability and function.

Silk fibroin (SF) from the domesticated silkworm *Bombyx mori* is a natural protein that has been of interest in biotechnology and biomedical applications due to its biocompatibility, ease of purification and processability into a variety of material formats including fibers, films, sponges

and gels. [48-50] Moreover, SF display excellent mechanical properties owing to natural self-assembly into crystalline β-sheets. [51, 52] This makes SF a more promising tough nanocoating material compared to gelatin, which displays inferior mechanical properties at physiological temperatures due to conformational transition above 20ºC and rapid enzymatic degradation [53]. However, SF has only a weak net negative charge [54] and therefore cannot be deposited directly on cell surface due to electrostatic repulsion. The synthesis of silk constructs with sufficient net charge for electrostatic LbL deposition was demonstrated by our group before through covalent conjugation of PL or PG [55]. SF-PL and SF-PG conjugates were used for the synthesis of pH-responsive hollow capsules [56, 57] or nanocoating of bacteria [58] or yeast [56], but not mammalian cells. Besides the conjugation of PL, SF can also be cationized by the amination of aspartic (Asp) and glutamic acid (Glu) side chains through carbodiimide coupling of ethylenediamine (EDA) as reported before for bovine serum albumin [59] and gelatin [19, 60, 61]. Considering the negative influence of high charge density on the cytotoxicity of polycations [38], cytocompatible silk polycations with a low charge density can be achieved thanks to significantly lower content of Asp and Glu (1.1 mol%) of SF [54] compared to gelatin (12.4 mol%). [62] Carboxylic acid content of SF can easily be increased if needed by the carboxylation of tyrosine [63] or serine groups [55] to tune its overall charge density and optimize the efficiency of electrostatic aggregation on charged substrates.

Herein we present the synthesis and characterization of cytocompatible silk ionomers for LbL electrostatic deposition on the plasma membrane of individual living mammalian cells. Our preliminary findings showed that SF-PL constructs were cytotoxic to mammalian cells and could not be used for nanoencapsulation. As an alternative, we demonstrated the synthesis of aminated silks with significantly lower charge density through carbodiimide coupling of EDA groups on pristine or carboxylated SF and obtained a library of silk-based polycations with varying charge

densities and molecular weight (MW) distributions. Aminated SF paired with carboxylated SF formed nanoscale multilayers on mammalian cells through electrostatic assembly. By the optimization of ionomer properties and the composition of incubation buffers, L929 murine fibroblasts and bone marrow-derived hMSCs were nanocoated successfully without significantly impairing their viability. To our knowledge, this study is the first to introduce silk-based cytocompatible polyelectrolytes that are suitable for nanoencapsulation of individual mammalian cells. Furthermore, here we provide a novel formulation of an incubation buffer for LbL assembly of multilayers on mammalian cells, which can be utilized for other polyelectrolyte materials with relatively low charge densities.

Experimental Section

Materials. p-toluene sulfonic acid, sodium nitrate, 4-aminobenzoic acid, chloroacetic acid, ethylenediamine dihydrochloride, 1-Ethyl-3-(3-dimethylaminopropyl) carbodiimide (EDC), N-hydroxy succinimide (NHS), 2,4,6-trinitrobenzene sulfonic acid (TNBSA), 4-(2-hydroxyethyl)-1-piperazineethanesulfonic acid (HEPES), dextrose and fluorescein isothiocyanate (FITC) isomer I were purchased from Sigma Aldrich, St. Louis, MO. 2-(N-morpholino)ethanesulfonic acid (MES) saline and sodium borate buffer packs, phosphate buffered saline (PBS), Dulbecco's Modified Eagle's Medium (DMEM), fetal bovine serum albumin (FBS) and Penicillin/Streptomycin (Pen-Strep) were from Thermo Fisher Scientific, Rockford, IL.

Extraction of silk fibroin (SF). *Bombyx mori* silkworm cocoons were degummed to remove sericin protein by boiling 5 g of cut cocoons in 2 L of 0.02 M sodium carbonate solution for 1, 60, 90 or 120 min and rinsing three times in deionized (DI) water. Degummed fibers were dried overnight and solubilized in 9.3 M lithium bromide solution at a concentration of 20% (w/v) for 4 h at 60°C. The solution was dialyzed against distilled water with 6 water changes over 3 days and

left in dialysis bag in a fume hood for 2 days to increase SF concentration through water evaporation. The resulting solution was centrifuged 2 times at 9,000 rpm at 4°C for 20 min to remove insoluble particles. The concentration of silk solution was determined by weighing a known volume of sample before and after drying overnight at 60°C.

Carboxylation and amination of SF. For the carboxylation of tyrosine groups, 4-aminobenzoic acid was diazonium coupled on phenol side chains as reported before. [63] Briefly, 34 mg of 4-aminobenzoic acid dissolved in 1.25 mL of acetonitrile was mixed with 625 µL of ice cold 0.8 M aqueous $NaNO_2$ and 625 µL of 1.6 M p-toluenesulfonic acid, vortexed and incubated on ice for 15 min. 1.5 mL of the diazonium salt solution was mixed with 2 mL of 10% w/v aqueous SF solution prepared in 0.5 M borate buffer (pH 9.0) and incubated on ice for 20 min. For the carboxylation of serine side groups thorough nucleophilic substitution reaction with chloroacetic acid as demonstrated before [55], 0.6% w/v SF was prepared in 1 M aqueous chloroacetic acid solution at pH ~13.5 and the mixture was stirred at room temperature (RT, 24°C) for 1 h. After dissolving NaH_2PO_4 to a final concentration of 4 mg/mL and bringing the pH of the solution to 7.4 with 10 M HCl, the solution was mixed for 30 min at RT. Tyrosine- (SF(Y)COOH) or serine-carboxylated SF (SF(S)COOH) solutions were then loaded into 3.5 kDa cutoff dialysis tubing and dialyzed against DI water for 4 days with 8 water changes. Solutions were centrifuged twice at 9000 rpm at 4°C to remove insoluble particles and then frozen at -80°C overnight, lyophilized and stored at -20°C until further use.

Serine-carboxylated silk was carbodiimide coupled with PL_{10} or PG_{10} for the analysis of silk-polyelectrolyte conjugates (SI experimental section). Cationized silks with lower charge density were synthesized through amination of unmodified or carboxylated silks through carbodiimide-coupling of ethylenediamine (EDA). Briefly, 2% w/v unmodified or carboxylated silks were

reacted with EDA dihydrochloride (1.5 g per 1 g SF) in the presence of EDC (850 mg per 1 g SF) and NHS (275 mg per 1 g SF) in 0.05 M MES buffer (pH 6.0) for 18 h at RT under gentle stirring. The solution was then dialyzed against DI water in 3.5 kDa cutoff dialysis tubing for 5 days with 10 water changes. Solutions were centrifuged twice at 9000 rpm at 4°C to remove insoluble particles and then frozen at -80°C overnight, lyophilized and stored at -20°C until further use.

Quantification of carboxylic acid and primary amine groups. Carboxylic acid content of the ionomer constructs was estimated by quantification of free protons through the measurement of solution pH after mixing with excess HCl solution. 0.05 M aqueous HCl was standardized by titration with 0.05 M standard NaOH solution in the presence of phenolphthalein. 2 mL of 5 $mg.mL^{-1}$ ionomer solution (n=3) was first mixed with 40 µL of 0.05 M NaOH to bring the pH to 6.5-7 if necessary for the complete deprotonation of the carboxylic acid residues. 2 mL of 0.05 M aqueous HCl was then added to the solution to bring pH to 1.5-2 and stirred for 15 min at RT for the complete protonation of carboxylic acid residues. The concentration of excess acid was then determined by measuring the solution pH using a pH-meter. The carboxylic acid contents of the carboxylated and aminated silks were calculated using the equations (1) and (2), respectively:

$$n_{COOH} \text{ / mg protein} = \frac{\left((V_1 * 10^{-pH_1}) + (0.002 * M_{HCl}) - (V_2 * 10^{-pH_2})\right) * 10^9}{10\ mg} \quad (1)$$

$$n_{COOH} \text{ / mg protein} = \frac{\left((0.002 * M_{HCl}) - (V_1 * 10^{-(14-pH_1)}) - (V_2 * 10^{-pH_2})\right) * 10^9}{10\ mg} \quad (2)$$

where n_{COOH} is the moles of carboxylic acid residues (in nmol), M_{HCl} is the concentration of the standardized HCl solution, V_1 and V_2 are the volumes (in liters) and pH_1 and pH_2 are the pH of the ionomer solutions before and after mixing with 2 mL of aqueous HCl solution, respectively. TNBSA assay was used to quantify the primary amine content of the ionomers. 0.5 mg/mL

ionomer solution was mixed with 0.05% w/v TNBSA solution in 0.4 M $NaHCO_3$ buffer (pH 8.5) at 1:1 volume ratio, incubated at 37°C for 2 h and its absorption at 420 nm was measured (n = 5) using SpectraMax M2 multi-mode microplate reader (Molecular Devices, Sunnyvale, CA). OD_{420} values were normalized to dye only and no dye controls and then converted to primary amine content (nmol/mg protein) using the calibration curve prepared with known concentrations of β-alanine standard solutions (**Supplementary Figure S1A**). Assuming complete deprotonation and protonation of carboxylic acid and primary amine residues, respectively, at pH 7.4, net charge of the silk ionomers was calculated using equation (3):

$$\text{Net charge (nmol/mg protein)} = n_{NH_2} - n_{COOH} \quad (3)$$

Zeta potential measurement. To determine the zeta potential of carboxylated and aminated silks, 5 $mg.mL^{-1}$ solutions were prepared in deionized (DI) water, the solution pH was brought to 7.4 and it was syringe-filtered through 0.22 μm filters. To determine the surface zeta potential of L929 fibroblasts during LbL nanocoating, cells were suspended in 40 mM HEPES buffer at a density of $2x10^5$ $cells.mL^{-1}$. Electrophoretic mobilities of ionomers or cells (n = 3) were measured using a NanoBrook ZetaPALS (Brookhaven Instruments, Holtsville, NY) and the zeta potential values were determined using the Smoluchowski model.

Analysis of molecular weight (MW) distribution. MW distribution of the silk constructs was semi-quantified on the digital images of SDS polyacrylamide gel electrophoresis (PAGE). 20 μL of samples and 10 μL of NOVEX sharp pre-stained protein standard were run in NuPAGE 4-12% Bis-Tris gels (Invitrogen, Carlsbad, CA) at 200 V for 30 min and stained with colloidal blue for 4 h. After rinsing overnight in DI water, gels were imaged, and the molecular weight distributions were determined using ImageJ (1.48v, NIH, USA) as reported before [53]. Briefly, a calibration curve was prepared by the digital analysis of reference ladder lane to obtain a linear equation for

conversion of the distance from wells to MW values. Frequency of each MW was then calculated from the mean grey values and MW distributions were plotted for each sample to determine the mean and peak molecular weights.

LbL deposition of silk ionomers on cell surface. L929 fibroblasts from mouse subcutaneous connective tissues or bone marrow-derived hMSCs (ATCC, Manassas, VA) were incubated in 1 $mg.mL^{-1}$ solution of aminated silk in 1X Dulbecco's Modified Eagle Medium (DMEM) or 40 mM HEPES buffer supplemented with 5% w/v dextrose and 50 mM NaCl (HD50) at a density of $2x10^6$ (L929) or $1x10^6$ $cells.mL^{-1}$ (hMSCs) for 1 min under gentle pipetting. Cells were then collected by centrifugation at 1500 rpm for 5 min at 4°C and washed with blank buffer. For the deposition of the second layer, cells were incubated in 1 $mg.mL^{-1}$ of carboxylated silk solution for 1 min, centrifuged and washed. The alternating incubation in aminated and carboxylated silk solutions was repeated to deposit 3 bilayers on the cells (n=3). Silk-nanocoated cells were seeded on TCP at a density of 10^4 $cells.cm^{-2}$ and incubated in DMEM supplemented with 10% FBS and 1% Pen-Strep at 37°C with 5% CO_2.

Cell viability and metabolic activity. Cells were stained with Live/Dead assay kit (Invitrogen, Carlsbad, CA) 2 h after seeding and imaged at days 1, 3 and 8 with a BZ-X700 Fluorescence Microscope (Keyence Corp., Itasca, IL). 5 random images were taken from 2h samples (n=3) and analyzed using live/dead staining macro of ImageJ to estimate the % viability of the nanocoated cells. Metabolic activity of the cells was monitored at days 1, 3, 5 and 8 by determining the % dye reduction (n=4) using alamarBlue viability assay (Invitrogen, Carlsbad, CA) according to the instructions by the manufacturer.

Confocal Laser Scanning Microscopy (CLSM). Carboxylated and aminated silks were fluorescently labeled with FITC to visualize nanolayer deposition on cell surface. Briefly, FITC

was dissolved in DMSO at a concentration of 10 mg/mL, diluted 4 times with DI water and 100 µL of it was added dropwise to 10 mL of 5 $mg.mL^{-1}$ solution of silk ionomers in 0.1 M carbonate buffer (pH 9.0). The mixture was stirred for 1 h at RT and then dialyzed in 3.5 kDa cutoff dialysis membranes against DI water for 3 days with 6 water changes. Solutions were frozen overnight, lyophilized, and stored at -20°C. Fluorescence emission by 0.1 $mg.mL^{-1}$ of FITC-labeled ionomer solutions at excitation / emission wavelengths of 488 nm / 520 nm was converted to FITC concentration / mg protein using a calibration curve obtained with known concentrations of FITC solutions (**Fig.S1B**). L929 cells and hMSCs were LbL nanocoated with FITC-labeled SF ionomers and visualized at 2h after seeding and at days 1, 3 and 8 using a TCS SP8 microscope from Leica Microsystems (Wetzlar, Germany) at excitation and emission wavelengths of 488 nm/500-540 nm. Relative fluorescence intensity of silk ionomer layers deposited on individual cells was quantified by mean gray values on Day 0 confocal images using ImageJ.

Scanning Electron Microscopy (SEM). Plastic coverslips were seeded with nanocoated L929 fibroblasts at a density of 10^4 $cells.cm^{-2}$ and incubated in growth media for 10 h at 37°C. After gently rinsing with 1X PBS, samples were fixed in 4% paraformaldehyde solution in PBS for 15 min at RT and washed with 40 mM HEPES buffer. After dehydration using a series of 50, 70 and 100% v/v ethanol solutions for 5 min, samples were Au-Pd coated under vacuum and examined under SEM (Zeiss EVO MA10, Germany).

Quartz Crystal Microbalance with Dissipation Monitoring (QCM-D) Analysis. LbL deposition of aminated and carboxylated silks was monitored using a Q-sense E4 QCM (Biolin Scientific, Sweden). Prior to measurement, QSX301 gold sensors were UV/ozone treated for 10 min followed by incubation in piranha solution (97% H_2SO_4:30% H_2O_2 = 3:1 v/v) for 5 min to clean and put negative charges on the sensor surface. After drying under N_2 flow, sensors were

placed into flow modules and washed with 1 $mg.mL^{-1}$ solutions of silk ionomers in DMEM or HD50 buffer for 10 min at a flow rate of 150 µL/min using a peristaltic pump. After each layer, the sensor was rinsed with blank buffer for 5 min to remove loosely bound silk chains.

Statistics. All data are expressed as mean ± standard deviation for $n \geq 3$. GraphPad Prism (GraphPad Software, La Jolla, CA) was used to perform One- or Two-way analysis of variance (ANOVA) with Tukey's post hoc multiple comparison test to determine statistical significance (*$p \leq 0.05$, **$p \leq 0.01$, ***$p \leq 0.001$). Correlation of two variables were analyzed using simple linear regression test to obtain a linear equation ($R^2 > 0.95$) for calibration curves used in quantification of primary amine contents by TNBSA assay, FITC concentration by fluorescence emission, and molecular weight distributions by SDS PAGE.

Results and Discussion

We synthesized negatively and positively charged SF ionomers through the conjugation of polyelectrolytes PL and PG or through the carboxylation and amination reactions to enable ionic pairing on plasma membrane for nanoencapsulation of living mammalian cells. Deposition of multiple SF-PL / SF-PG layers on living yeast cells or the bacterial strains *E. coli* and *B. subtilis* were reported before with cell viabilities of 38% [56] and between 15-50% [58], respectively. Since LbL deposition of SF-polyelectrolytes on a mammalian cell line has not been demonstrated before, we first investigated the cytocompatibility of the process on mouse fibroblasts. SF was serine-modified with PL_{10} or PG_{10} (**Fig.S2A**) and characterized prior to cell surface deposition. As expected, the primary amine content of SF increased significantly from ~400 to ~3,000 nmol/mg protein upon modification with PL (**Fig.S2B**). SF(S)-PL had a positive zeta potential ~ +20 mV) while unmodified SF (~ -10 mV), SF(S)COOH and SF(S)-PG (~ -20 mV) had negative zeta potentials (**Fig.S2C**). For the electrostatic deposition of the first layer on negatively charged cell

surface, we first incubated the cells with positively charged SF(S)-PL and then with negatively charged SF(S)-PG (**Fig.S2D**). Cells were positive for fluorescent signal after incubation with FITC-labeled SF(S)-PL (**Fig.S2E**), suggesting its aggregation on cell membrane. After incubation in 1 $mgmL^{-1}$ solutions of SF(S)-PL_{10} in 1X PBS or DMEM for 1 min, cell viability decreased below 20% with or without the deposition of a negatively charged SF(S)-PG_{10} layer (**Fig.S2F, G)**, indicating cytotoxicity of PL chains conjugated on SF. Despite a few studies that showed nanocoating of mouse or human MSCs with multiple bilayers of PL and HA without significant effect on cell viability, [3, 16] others also reported survival rates below 30% when PL was used as the polycation layer. [17, 38, 39] The extent of cytotoxicity depends on the charge density, molecular weight or concentration of polycations [38]; therefore, we focused on the optimization silk ionomer structure and chemistry as well as the incubation conditions to achieve LbL nanocoating with minimum cytotoxicity.

A library of carboxylated and aminated silk constructs with varying charge densities and MW distributions were synthesized for LbL nanocoating of mammalian cells by first incubating them in in aminated and then carboxylated silk solutions for electrostatic LbL deposition on negatively charged plasma membrane (**Fig.1A**). Regenerated SF molecules were carboxylated on tyrosine (5.3 mol%) or serine (12.1 mol% [54]) residues (**Fig.1B**) to increase the carboxylic acid content for carbodiimide coupling as well as the net negative charge. To achieve different positive charge densities, EDA was coupled on unmodified SF (**Fig.1C-i**), SF(Y)COOH (**Fig.1C-ii**) or SF(S)COOH (**Fig.1C-iii**). Carboxylation and amination of SF were monitored by ^{1}H NMR (**Fig.S3**). Diazonium coupling introduced two new peaks (7.26, 7.68 ppm) in the aromatic region of SF(Y)COOH proton spectrum. Methylene proton signals of the acetic acid residues on SF(S)COOH were expected at around 4.1 - 4.3 ppm but could not be observed clearly, likely

because of overlaps with Alaα/Serα proton peaks at 4.14-4.29 ppm. Alkyl proton peaks of EDA appeared next to Tyr β proton peaks between 2.4-3.2 ppm on the spectrum of all aminated silks, indicating successful conjugation of EDA on unmodified or carboxylated silks.

We obtained different MW constructs by varying the duration of degumming. The MW of the intact SF heavy chain is ~390 kDa, which decreases with increasing degumming time due to protein degradation. [64] SF degummed for 60, 90 or 120 minutes were carboxylated and aminated and their MW distributions were digitally quantified on SDS-PAGE images (**Fig.S4A**) using the calibration curves obtained from the reference ladder lanes (**Fig.S4B**). The peak MW of SF extracted by degumming for 60, 90 and 120 minutes were 131 kDa, 98 and 81 kDa, respectively, and became 108, 110 and 100 kDa, respectively, after tyrosine carboxylation (**Fig.2A**, **Table 1**). Diazonium coupling of aminobenzoic acid was shown to increase the hydrophobicity of silk [63]. Thus, the decrease in MW of 131 kDa SF upon tyrosine carboxylation could be due to insoluble aggregates that were removed by centrifugation after dialysis. The most significant change in MW distribution was observed for serine-carboxylated SF. The peak MW of 131 kDa SF dropped to 36 kDa after serine-carboxylation, indicating a more than a 3-fold decrease (**Table 1**). This could be explained with the alkaline hydrolysis of amide bonds [65] within the SF backbone at highly alkaline pH (~13.5) used for deprotonation of serine groups (pK_a ~13.0) [66] during nucleophilic substitution reaction with chloroacetic acid. We decreased the duration of degumming to 1 minute to obtain a higher molecular weight serine-modified silks and assess its influence on cytocompatibility. Indeed, higher MW constructs were obtained as the peak MWs of 1 minute degummed silk was ~64 kDa (**Fig.2A)** after serine-carboxylation. However, it should be noted that a minimum of ~30 min degumming is required for complete the removal of sericin [67], which comprises 20-30 wt.% of raw silk fibers [64] and has significantly higher contents of Ser (~26 mol%), Asp (~18 mol%) and

Glu (~6 mol%) [68] compared to fibroin heavy chain (12.1, 0.5 and 0.6 mol%, respectively [54]). Therefore, 64 kDa SF(S)COOH samples likely contained residual sericin and had a different amino acid composition compared to sericin-free 36 kDa SF(S)COOH. After amination with EDA, peak MW of unmodified SF slightly decreased, while it increased slightly for serine-carboxylated SF and drastically for tyrosine-carboxylated SF (**Fig.2B, Table 1**). The solubility of all lyophilized SF(Y)-EDA constructs was also significantly lower compared to SF(Y)COOH counterparts (data not shown), suggesting intra- and interchain crosslinking despite high molar excess of EDA used during amination. This was likely due to the carboxylation of tyrosine residues in the repetitive hydrophobic domains that can self-assemble into crystalline β-sheets. [69, 70] The increased hydrophobicity of SF by coupling of benzoic acid residues [63] combined with enhanced pi-stacking interactions by diazonium groups [71] might have induced packing of the repetitive domains in aqueous solution, leading to crosslinking of adjacent carboxylic acid residues during carbodiimide coupling of EDA (**Fig.S5A**). In the case of SF(S)COOH, on the other hand, significant reduction in MW and the conjugation of hydrophilic acetic acid groups on serine side chains located in the hydrophobic domains likely limited hydrophobic interactions and therefore intra- and interchain crosslinking (**Fig.S5B**).

To assess the charge profiles of carboxylated and aminated silk constructs, we determined the concentrations of carboxylic acids and primary amines as well as the zeta potentials of silk ionomers. Considering that the pK_a values of Asp and Glu side chains and the acetic and benzoic acid residues range between 3-5 [72-74], we brought the pH of ionomer solutions between 1.5-2 to quantify excess acid by pH measurement after complete protonation of all carboxylic acid residues. The main limitation of the approach was, however, the precipitation of unmodified and tyrosine-carboxylated silks at low pH (**Fig.S6**), likely through self-assembly of water-insoluble β-sheets

upon carboxylation of the carboxylic acid residues [75, 76]. Diazonium carboxylation of SF was reported to decrease the tendency of spontaneous β-sheet formation but do not prevent crystallization by pH reduction [63], which is parallel with our observations. Unlike SF or SF(Y)COOH, SF(S)COOH did not precipitate at low pH (**Fig.S6**), suggesting that the drop in MW together with the carboxylation of Ser residues in hydrophobic domains downregulated self-assembly of crystalline β-sheet structures as reported before [77]. None of the aminated silks including SF(Y)-EDA precipitated at low pH despite the increase in MW compared to carboxylated counterparts, indicating a shift in SF pK_a from acidic to alkaline region as expected upon conversion of carboxylic acid residues into basic primary amine groups. Both carboxylic acid (**Fig.S7A**) and primary amine concentration (**Fig.S7B**) of unmodified SF decreased gradually with increasing mean MW (**Table S1**) as expected because of more free N- and C- termini created upon hydrolysis into shorter chains during degumming. The empirical concentrations were significantly higher than the theoretical values, suggesting that there were many more N- and C-termini than those calculated based on mean MW. Although the carboxylation of tyrosine and serine residues increased the total carboxylic acid content significantly compared to unmodified silk, the yield of carboxylation was in the range of only 20-35% (**Table S1**), likely because of the poor accessibility Ser and Tyr in the hydrophobic domains [69, 70]. Besides increasing the carboxylic acid content, serine carboxylation also increased the concentration of primary amines significantly because of protein hydrolysis and formation of new N-termini during the reaction. Interestingly, primary amine content decreased after diazonium coupling on tyrosine residues (**Fig.3A-i**), likely due to deamination upon reaction with excess nitrous acid [78]. For diazonium coupling, we used 2X molar excess of $NaNO_2$ (~0.5 mmol) than 4-aminobenzoic acid (~0.25 mmol) based on our previous report [63]. The nitrites in acidic solution probably reacted with the primary amines and formed N-

nitrosamines, which are rapidly converted into diazoic acids and decompose by N_2 gas release in aqueous environment [79]. As expected, primary amine content of all silk constructs increased from 50 – 400 to 400 – 770 nmol/mg protein (**Fig.3A-ii**) after EDA conjugation, indicating successful amination of SF. Among all aminated SF constructs, 70 and 39 kDa SF(S)-EDA had the highest primary amine content (~770 nmol.mg^{-1} protein), which was still significantly lower than SF(S)-PL (~3000 nmol/mg protein, **Fig.S1A**) as desired. The yield of amination was above 75% for SF-EDA constructs and above 55% for 226 kDa SF(Y)-EDA or 70 and 39 kDa SF(S)-EDA, while it was below 50% for 217 and 219 kDa SF(Y)-EDA. We estimated the net charge of the ionomers from the difference in empirical concentrations of carboxylic acid and primary amine residues (**Table 2**) and neglected the contribution by Arg and His side chains (~0.6 mol%). All carboxylated and aminated constructs had a a net negative and positive charge, respectively, as desired. The zeta potential of unmodified SF (~ -10 mV) became more negative (~ -25 mV) upon tyrosine- or serine-carboxylation (**Fig.3B-i**), and positive after coupling of EDA (**Fig.3B-ii**), further confirming successful carboxylation and amination of SF. Despite having a comparable charge concentration with the SF-EDA constructs or 70 kDa SF(S)-EDA, 39 kDa SF(S)-EDA had the highest positive zeta potential at around +34 mV, likely because of having the lowest peak MW that resulted in significantly lower hydrodynamic radius and therefore higher electrophoretic mobility of ionomer molecules in solution. [80]

We determined the cytocompatibility of aminated SFs with mammalian cells by live/dead assay using L929 murine fibroblasts. After incubation in aminated SF solutions in 1X PBS for 10 min, no significant change was recorded in cell viability for SF-EDA or SF(Y)-EDA irrespective of the protein concentration (1 - 10 mg.mL^{-1}) while SF(S)-EDA constructs were highly cytotoxic above 1 mgmL^{-1} (**Fig.S8**). Despite having comparable primary amine contents, 70 kDa SF(S)-EDA

solution displayed higher cytotoxicity than its 39 kDa counterpart, the former and latter resulting in cell viabilities of 62% and 89%, respectively. This could be due to 70 kDa SF(S)-EDA having a higher peak MW than 39 kDa SF(S)-EDA. Indeed, higher MW polycations displaying higher cytotoxicity compared to lower MW counterparts was reported before with L929 fibroblasts incubated in various MW of diethylaminoethyl (DEAE)-dextran [38]. To visualize silk deposition on cell membranes, cells were incubated in solutions of FITC-labeled silk polycations. The quantification of FITC-labeling revealed that all aminated silks except SF(Y)-EDA were strongly positive for FITC (**Fig.S9A-i**). A low FITC content was recorded for 226 kDa SF(Y)-EDA, while it was negligible for 217 or 219 kDa SF(Y)-EDA counterparts. A potential explanation for low FITC signal on tyrosine-modified constructs could be the coloration of SF upon coupling of azo groups [63] that might have competed for light absorption or quenched the emission by FITC. Indeed, we observed a shoulder in the absorption spectra of SF(Y)-EDA constructs, particularly in those of 217 and 219 kDa (**Fig.S9A-ii**), that might have overlapped with the excitation wavelength of FITC at 488 nm. No FITC signal was collected from the cells incubated in PBS solutions of SF-EDA or 226 kDa SF(Y)-EDA even at 10 mg.mL^{-1}, whereas the cells incubated in 1 mgmL^{-1} SF(S)-EDA solutions were positive for fluorescence signal (**Fig.S9B**). This could be explained with significantly higher primary amine content of SF(S)-EDA constructs that likely allowed for better competition with other cationic species available in PBS for the negatively charged cell membrane. **Fig.S9C** clearly shows that the success of deposition increased while cell viability decreased with increasing primary amine content of positively charged silk ionomer constructs when PBS was used as the incubation buffer. The cytotoxicity was alleviated successfully by reducing the overall charge density through the conjugation of EDA instead of PL on serine-carboxylated silks.

100 kDa SF(Y)COOH and 64 kDa SF(S)COOH were chosen as negatively charged layers for LbL nanocoating to determine if the charge and the chemistry of silk polyanion affects cell viability. When coupled with SF-EDA or SF(S)-EDA constructs, 100 kDa SF(Y)COOH and 64 kDa SF(S)COOH provided negative to positive charge ratios of around 0.92 and 0.58, respectively (**Table 2**). Despite cell survival above 60% when coated with a single SF(S)-EDA layer, no cells survived after LbL deposition of multilayers in PBS irrespective of the type of carboxylated silk or incubation time (**Fig.S7A**). When PBS was replaced with DMEM growth media, which includes divalent Ca^{2+} and Mg^{2+} ions as well as basic amino acids in addition to Na^{+} and K^{+} (**Table S1**), cell viability increased significantly to above 90%, particularly when 64 kDa SF(S)COOH was used as the negatively charged silk (**Fig.S10A**). Divalent cations had a higher charge density than monovalent cations and were shown to hinder electrostatic aggregation of polyelectrolytes on cell surface to a higher degree [21, 39]. Indeed, FITC signal from the ionomer layers decreased compared to PBS (**Fig.S10B**), suggesting a decrease in the yield of deposition. To enhance the cell surface-deposition of SF-EDA and SF(Y)-EDA with lower charge densities than SF(S)-EDA, we formulized a new cation-free incubation buffer at pH 7.4 by supplementing 5% w/v dextrose solution, which was shown to display suitable osmolarity for the short-term incubation of human MSCs [81], with 40 mM HEPES. Cell viability decreased significantly after incubation in HEPES-Dextrose (HD) solutions of SF-EDA and no cells survived in the solutions of SF(S)-EDA (**Fig.S11A**). Since the survival rate of the control cells was around 89%, higher cytotoxicity could be attributed to improved electrostatic aggregation of the aminated silks on the cells in the cation-free buffer. Indeed, cell surfaces were positive for FITC signal after incubation in HD solutions of 123 or 85 kDa SF-EDA at both low and high concentration (**Fig.S11B**). The 75 kDa SF-EDA was deposited on the cells only at high concentration but resulted in a survival rate of ~50%. 226 kDa

SF(Y)-EDA was deposited on the cells only at low concentration, likely due to its limited solubility at higher concentrations. Cell survival rate after deposition of (85 kDa SF-EDA / 100 kDa SF(Y)COOH)$_3$ in HD buffer was around 60%. To test whether it could be improved by tuning the ionic composition of the buffer, we supplemented HD buffer with NaCl at varying concentrations. Cell viability increased above 85% with 25 mM NaCl and above 90% with 50 or 100 mM NaCl in HD (**Fig.S12A, B**). The FITC signal on cell surfaces, however, faded gradually with increasing NaCl concentration (**Fig.S12C, D**), suggesting that increasing ionic strength of the incubation buffer hindered the electrostatic aggregation on cell surfaces. Although cell viability was preserved, no FITC signal was collected on cell surfaces after coating with (226 kDa SF(Y)-EDA / 100 kDa SF(Y)COOH)$_3$ in HD or HD50 buffers (data not shown). We concluded that the amination of tyrosine-carboxylated constructs was not effective likely due to deamination by nitrous acid during diazonium coupling as well as intermolecular crosslinking during carbodiimide coupling of EDA. Therefore, this conduction was eliminated from the rest of the study.

Based on their performance in terms of cell viability and deposition on cell surfaces, LbL deposition was further investigated using SF-EDA and SF(S)-EDA constructs in HD50 and DMEM, respectively. As shown in **Fig.4A** and **Fig.S13A**, discrete FITC-positive layers surrounded the surfaces of the L929 fibroblasts or hMSCs, respectively. The viability of nanocoated cells was above 90% (**Fig.4B**) and 80% (**Fig.S13B, C**), respectively, which was not significantly different than the respective control groups, indicating cytocompatibility of the LbL nanocoating with aminated and carboxylated silks. The surface charge of L929 fibroblasts during LbL deposition of (123 kDa SF-EDA / 100 kDa SF(Y)COOH)$_3$ and (70 kDa SF(S)-EDA / 64 kDa SF(S)COOH)$_3$ was monitored by zeta potential measurement. pK_a values of phosphotidylserine head groups (~3.5) [82] and the sialic acid residues (~2.6) of membrane oligosaccharides and

glycoconjugates [83] are below 7, providing a negative zeta potential to mammalian cell surface ranging from -30 to -20 mV at physiological pH. [84, 85] Indeed, uncoated cells had a zeta potential ranging from -20 to -25 mV, which became positive upon deposition of the aminated silks and negative again after incubation in the carboxylated silk solution as expected. A zigzag pattern alternating between negative and positive zeta potential values (**Fig.5A**) was recorded for both groups during the deposition of 6 layers as in previous reports [16, 17, 19]. We visualized the nanocoated cells by brightfield microscopy and SEM after deposition of each bilayer. Contrary to the spread morphology of control cells, coated cells had a flake-like, relatively spherical shape with a rougher surface (**Fig.5B, Fig.S14)**, resembling morphologies demonstrated for neural stem cells (NSCs) and T cells after coating with gelatin/alginate [17] and chitosan/alginate bilayers [22], respectively. The thin layer of lamellipodia beneath the cells (**Fig.5B**, shown with black arrows) disappeared with increased numbers of bilayers, suggesting the formation of silk shells around the cells after deposition of 3 bilayers.

The LbL assembly of silk ionomers was investigated by QCM-D analysis. The resonance frequency of the oscillating quartz crystal decreased gradually with each silk ionomer layer (**Fig.6A**), indicating adsorption of mass onto sensor surface. [86, 87] A slight increase in frequency was recorded during each washing step, which could be attributed to the removal of loosely bound silk chains and reorganization of the ionomer molecules to a denser layer. The thickness and elastic moduli of the silk multilayers were estimated with the viscoelastic model using the individual frequency and dissipation shifts (**Fig.S15A**). A roughly linear increase in the multilayer thickness (R^2= 0.9947 and 0.9946 for 123 kDa SF-EDA / 100 kDa SF(Y)COOH and 70 kDa SF(S)-EDA / 64 kDa SF(S)COOH, respectively) was found during the deposition of 6 layers (**Fig.6B**). Despite the lower charge density of 123 kDa SF-EDA than 70 kDa SF(S)-EDA, a more robust decrease in

resonance frequency was recorded for the former than the latter, leading to estimated film thicknesses of ~142 and 126 nm, respectively. Moreover, DMEM had a higher ionic composition, which is known to increase the thickness of LbL assembled films by inducing coil formations in the polyelectrolyte chains prior to adsorption, as well as increasing water retention within the multilayers. In lower ionic strength solutions, on the other hand, thinner multilayers are expected because of flatter orientation of the polyelectrolytes parallel to the surface and water release from the layers [88-90]. Higher thickness of (123 kDa SF-EDA / 100 kDa SF(Y)COOH) multilayers could be because of the higher MW and lower charge of the components than with the serine-modified ionomers, which might have led to a coiled conformation through self-assembly of the hydrophobic domains [91] even at low ionic strength. The elastic moduli of 3 bilayers were estimated as ~660 and 840 kPa for (123 kDa SF-EDA / 100 kDa SF(Y)COOH) and (70 kDa SF(S)-EDA / 64 kDa SF(S)COOH) multilayers (**Fig.S15B**), suggesting that the latter formed a thinner and more rigid film on the electrode than the former.

The persistence of the silk shells encapsulating the cells was monitored over time by CLSM imaging of the cells coated with FITC-labeled ionomers. The discrete circular silk layers surrounding the cells disappeared by day 1 and the FITC signal completely diminished by day 8 for both (123 kDa SF-EDA / 100 kDa SF(Y)COOH)$_3$ and (70 kDa SF(S)-EDA / 64 kDa SF(S)COOH)$_3$ shells (**Fig.7A**). Fluctuations in solution pH is known to affect the stability of polyelectrolyte bilayers by altering net charges and disrupting ionic bridges [92]. Although the metabolic activity may slightly alter the pH of growth media, extracellular pH of viable cells should be in between 6.5-8 [93]. Within this range we did not expect a significant change in the sign of electric charges, or the integrity of ionomer bilayers. Therefore, the rapid release of the cells from silk nanocoatings could be explained with the endocytosis of polyelectrolyte bilayers [16, 17,

[45] as well as the gradual dissociation of multilayers by ongoing ion exchange [94, 95] in growth media through to the competition for aminated/carboxylated silk ion pairs by external ionic species. One approach to prolong the lifetime of silk multilayers on the cells would be to lower the incubation temperature below 15°C to decrease the rate of endocytosis [96] and increase the number of bilayers deposited on cell surface to improve persistence. [18] Alternatively, high stability of multilayers could be achieved at physiological temperatures by covalent crosslinking of the bilayers as it was reported for multilayers of cationized and anionic gelatin using transglutaminase [25]. Unlike other polyelectrolytes, silk ionomers can also be crosslinked covalently by horseradish peroxidase (HRP) [53] or Fenton reaction-mediated [97] dityrosine bridging in the presence of low concentrations of hydrogen peroxide (H_2O_2) or physically through the self-assembly of hydrophobic domains into crystalline β-sheets in the presence of polyalcohols such as PVA, PEG or glycerol. [98] Dissociation of silk nanocoatings from the cell surface could be delayed through covalent or physical crosslinking of ionomer bilayers, which will be investigated in our future studies.

Live/dead staining of the cells demonstrated an increase in the density of the nanocoated cells from day 1 to day 8 (**Fig. 7B**), and the metabolic activity estimated by percent reduction of alamarBlue gradually increased over 8 days for both control and coated cells (**Fig.7C**), indicating cell proliferation. Dye reduction by the nanocoated cells, particularly the (123 kDa SF- EDA / 100 kDa $SF(Y)COOH)_3$ group, was significantly lower than the control cells at days 1 and 3, which suggests lower metabolic activity and proliferation at early time points. The impaired proliferation of nanocoated mammalian cells was also documented before by others, and it was explained with physical hinderance of cell division as well as the interaction with environmental cues by the shell surrounding the cell membrane. [11, 15]

Conclusions

Simple one or two step chemistries were utilized to increase the carboxylic acid or primary amine content of SF to obtain negatively or positively charged silk-based polyelectrolytes, respectively. Covalent conjugation of EDA residues instead of PL on unmodified and tyrosine- or serine-carboxylated SF of varying MW distributions allowed for the synthesis of a library of silk polycations that had significantly lower charge density and improved cytocompatibility compared to SF-PL constructs. The net charge of cell surfaces was manipulated through the electrostatic deposition of aminated and carboxylated silks on living cells. Through the optimization of the ionic composition of incubation buffers and the duration of incubation in silk ionomer solutions, mouse fibroblasts and hMSCs were successfully nanocoated with multiple layers of silk ionomers without a significant reduction in cell viability. Cell encapsulating silk ionomer shells were transient and rapidly disappeared under culture conditions, allowing for release and proliferation of nanocoated cells. The results reported here establish a new and facile approach to coating otherwise sensitive mammalian cells. With the versatile options to modulate the biophysical and chemical features of the silk materials used, combined with the robust material properties and biocompatibility of the protein, future directions can be explored related to the utility of these systems in a range of biomedically-relevant directions.

Supporting Information:

Experimental details, detailed silk-polyelectrolyte and silk ionomer characterization, explanatory schematics, LbL deposition and cytotoxicity measurements with hMSCs, additional confocal and SEM micrographs

Author Information

ORCID

Onur Hasturk: 0000-0002-0030-8967

Jugal K. Sahoo: 0000-0003-2503-9115

David L. Kaplan: 0000-0002-9245-7774

Notes:

The authors declare no competing financial interest.

Acknowledgements

This work was supported by the NIH (P41EB027062, R01EB021264, R01NS094218, R01AR070975) and the U.S. Air Force (FA9550-17-1-0333 FA8650-15-D-5405). We also acknowledge the Turkish Fulbright Commission for PhD fellowship of O.H.

References

[1] Granicka, L. H. Nanoencapsulation of cells within multilayer shells for biomedical applications. *J. Nanosci. Nanotechnol.* **2014,** 14(1), 705-716.

[2] Hasturk, O.; Kaplan, D. L. Cell armor for protection against environmental stress: Advances, challenges and applications in micro-and nanoencapsulation of mammalian cells. *Acta Biomater.* **2019,** 95, 3-31.

[3] Choi, D.; Park, J.; Heo, J.; Oh, T. I.; Lee, E.; Hong, J. Cytoprotective self-assembled RGD peptide nanofilms for surface modification of viable mesenchymal stem cells. *ACS Appl. Mater. Interfaces* **2017,** 9(14), 12264-12271.

[4] Matsuzawa, A.; Matsusaki, M.; Akashi, M. Effectiveness of nanometer-sized extracellular matrix layer-by-layer assembled films for a cell membrane coating protecting cells from physical stress. *Langmuir* **2013,** 29(24), 7362-7368.

[5] Nishiguchi, A.; Yoshida, H.; Matsusaki, M.; Akashi, M. Rapid construction of three-dimensional multilayered tissues with endothelial tube networks by the cell-accumulation technique. *Adv. Mater*. **2011,** 23(31), 3506-3510.

[6] Amano, Y.; Nishiguchi, A.; Matsusaki, M.; Iseoka, H.; Miyagawa, S.; Sawa, Y.; Akashi, M. Development of vascularized iPSC derived 3D-cardiomyocyte tissues by filtration Layer-by-Layer technique and their application for pharmaceutical assays. *Acta Biomater.* **2016,** 33, 110-121.

[7] Liu, C. Y.; Matsusaki, M.; Akashi, M. The construction of cell-density controlled three-dimensional tissues by coating micrometer-sized collagen fiber matrices on single cell surfaces. *RSC Adv.* **2014,** 4(86), 46141-46144.

[8] Zheng, W.; Gao, J.; Song, L.; Chen, C.; Guan, D.; Wang, Z.; Yang, Z. Surface-induced hydrogelation inhibits platelet aggregation. *J. Am. Chem. Soc.* **2013,** 135(1), 266-271.

[9] Lee, J.; Cho, H.; Choi, J.; Kim, D.; Hong, D.; Park, J. H.; Choi, I. S. Chemical sporulation and germination: cytoprotective nanocoating of individual mammalian cells with a degradable tannic acid–Fe III complex. *Nanoscale* **2015,** 7(45), 18918-18922.

[10] Park, T.; Kim, J. Y.; Cho, H.; Moon, H. C.; Kim, B. J.; Park, J. H.; Choi, I. S. Artificial spores: Immunoprotective nanocoating of red blood cells with supramolecular ferric ion-tannic acid complex. *Polymers* **2017,** 9(4), 140.

[11] Yang, J.; Li, J.; Wang, X.; Li, X.; Kawazoe, N.; Chen, G. Single mammalian cell encapsulation by in situ polymerization. *J. Mater. Chem. B* **2016,** 4(47), 7662-7668.

[12] Kim, H.; Shin, K.; Park, O. K.; Choi, D.; Kim, H. D.; Baik, S.; Hyeon, T. General and facile coating of single cells via mild reduction. *J. Am. Chem. Soc.* **2018,** 140(4), 1199-1202.

[13] Sakai, S.; Taya, M. On-cell surface cross-linking of polymer molecules by horseradish peroxidase anchored to cell membrane for individual cell encapsulation in hydrogel sheath. *ACS Macro Lett.* **2014,** 3(10), 972-975.

[14] Sakai, S.; Liu, Y.; Sengoku, M.; Taya, M. Cell-selective encapsulation in hydrogel sheaths via biospecific identification and biochemical cross-linking. *Biomaterials* **2015,** 53, 494-501.

[15] Lee, J.; Choi, J.; Park, J. H.; Kim, M. H.; Hong, D.; Cho, H.; Choi, I. S. Cytoprotective silica coating of individual mammalian cells through bioinspired silicification. *Angew. Chem.* **2014,** 53(31), 8056-8059.

[16] Veerabadran, N. G.; Goli, P. L.; Stewart-Clark, S. S.; Lvov, Y. M.; Mills, D. K. Nanoencapsulation of stem cells within polyelectrolyte multilayer shells. *Macromol. Biosci.* **2007,** 7(7), 877-882.

[17] Li, W.; Guan, T.; Zhang, X.; Wang, Z.; Wang, M.; Zhong, W.; Kong, J. The effect of layer-by-layer assembly coating on the proliferation and differentiation of neural stem cells. *ACS Appl. Mater. Interfaces* **2015,** 7(5), 3018-3029.

[18] Choi, D.; Lee, H.; Kim, H. B.; Yang, M.; Heo, J.; Won, Y.; Lee, E. Cytoprotective self-assembled RGD peptide nanofilms for surface modification of viable mesenchymal stem cells. *Chem. Mater.* **2017,** 29(5), 2055-2065.

[19] Yang, J.; Li, J.; Li, X.; Wang, X.; Yang, Y.; Kawazoe, N.; Chen, G. Nanoencapsulation of individual mammalian cells with cytoprotective polymer shell. *Biomaterials* **2017,** 133, 253-262.

[20] Mansouri, S.; Merhi, Y.; Winnik, F. M.; Tabrizian, M. Investigation of layer-by-layer assembly of polyelectrolytes on fully functional human red blood cells in suspension for attenuated immune response. *Biomacromolecules* **2011,** 12(3), 585-592.

[21] Zhao, Q.; Li, H.; Li, B. Nanoencapsulating living biological cells using electrostatic layer-by-layer self-assembly: Platelets as a model. *J. Mater. Res.* **2011,** 26(2), 347-351.

[22] Zhao, S.; Zhang, L.; Han, J.; Chu, J.; Wang, H.; Chen, X.; Yearsley, M. Conformal Nanoencapsulation of Allogeneic T Cells Mitigates Graft-versus-Host Disease and Retains Graft-versus-Leukemia Activity. *ACS Nano* **2016,** 10(6), 6189-6200.

[23] Wang, J.; Miao, Y.; Huang, Y.; Lin, B.; Liu, X.; Xiao, S.; Xing, M. Bottom-up Nanoencapsulation from Single Cells to Tunable and Scalable Cellular Spheroids for Hair Follicle Regeneration. *Adv. Healthc. Mater.* **2018,** 7(3), 1700447.

[24] Li, W.; Zhang, G.; Guan, T.; Zhang, X.; Khosrozadeh, A.; Xing, M.; Kong, J. Manipulable Permeability of Nanogel Encapsulation on Cells Exerts Protective Effect against TNF-α-Induced Apoptosis. *ACS Biomater.-Sci. Eng.* **2018,** 4(8), 2825-2835.

[25] Sun, J.; Ren, Y.; Wang, W.; Hao, H.; Tang, M.; Zhang, Z.; Shi, X. Transglutaminase-catalyzed encapsulation of individual mammalian cells with biocompatible and cytoprotective gelatin nanoshells. *ACS Biomater.-Sci. Eng.* **2020,** 6(4), 2336–2345.

[26] Jiang, C.; Tsukruk, V. V. Freestanding nanostructures via layer-by-layer assembly. *Adv. Mater.* **2006,** 18(7), 829-840.

[27] Tang, Z.; Wang, Y.; Podsiadlo, P.; Kotov, N. A. Biomedical applications of layer-by-layer assembly: from biomimetics to tissue engineering. *Adv. Mater.* **2006,** 18(24), 3203-3224.

[28] Richardson, J. J.; Björnmalm, M.; & Caruso, F. Technology-driven layer-by-layer assembly of nanofilms. *Science* **2015,** 348(6233), aaa2491.

[29] Yang, S. H.; Hong, D.; Lee, J.; Ko, E. H.; Choi, I. S. Artificial spores: cytocompatible encapsulation of individual living cells within thin, tough artificial shells. *Small* **2013,** 9(2), 178-186.

[30] Park, J. H.; Hong, D.; Lee, J.; Choi, I. S. Cell-in-shell hybrids: chemical nanoencapsulation of individual cells. *Acc. Chem. Res.* **2016,** 49(5), 792-800.

[31] Kim, B. J.; Cho, H.; Park, J. H.; Mano, J. F.; Choi, I. S. Strategic advances in formation of cell-in-shell structures: From syntheses to applications. *Adv. Mater*. **2018,** 30(14), 1706063.

[32] Hong, D.; Park, M.; Yang, S. H.; Lee, J.; Kim, Y. G.; Choi, I. S. Artificial spores: cytoprotective nanoencapsulation of living cells. *Trends Biotechnol*. **2013,** 31(8), 442-447.

[33] Park, J. H.; Yang, S. H.; Lee, J.; Ko, E. H.; Hong, D.; Choi, I. S. Park, J. H., Yang, S. H., Lee, J., Ko, E. H., Hong, D., & Choi, I. S. (2014). Nanocoating of single cells: From maintenance of cell viability to manipulation of cellular activities. *Adv. Mater.* **2014,** 26(13), 2001-2010.

[34] Krol, S.; Del Guerra, S.; Grupillo, M.; Diaspro, A.; Gliozzi, A.; Marchetti, P. Multilayer nanoencapsulation. New approach for immune protection of human pancreatic islets. *Nano Lett.* **2006,** 6(9), 1933-1939.

[35] Zhi, Z. L.; Liu, B.; Jones, P. M.; Pickup, J. C. Polysaccharide multilayer nanoencapsulation of insulin-producing β-cells grown as pseudoislets for potential cellular delivery of insulin. *Biomacromolecules* **2010,** 11(3), 610-616.

[36] Ryan, A. J.; O'Neill, H. S.; Duffy, G. P.; O'Brien, F. J. Advances in polymeric islet cell encapsulation technologies to limit the foreign body response and provide immunoisolation. *Curr. Opin. Pharmacol.* **2017,** 36, 66-71.

[37] Oliveira, M. B.; Hatami, J.; Mano, J. F. Coating Strategies Using Layer-by-layer Deposition for Cell Encapsulation. *Chem.: Asian J.* **2016,** 11(12), 1753-1764.

[38] Fischer, D.; Li, Y.; Ahlemeyer, B.; Krieglstein, J.; Kissel, T. In vitro cytotoxicity testing of polycations: influence of polymer structure on cell viability and hemolysis. *Biomaterials*, **2003,** 24(7), 1121-1131.

[39] Germain, M.; Balaguer, P.; Nicolas, J. C.; Lopez, F.; Esteve, J. P.; Sukhorukov, G. B.; Fournier, D. Protection of mammalian cell used in biosensors by coating with a polyelectrolyte shell. *Biosens. Bioelectron.* **2006,** 21(8), 1566-1573.

[40] Mazia, D.; Schatten, G.; Sale, W. Adhesion of cells to surfaces coated with polylysine. Applications to electron microscopy. *J. Cell Biol.* **1975,** 66(1), 198-200.

[41] Hong, S.; Leroueil, P. R.; Janus, E. K.; Peters, J. L.; Kober, M. M.; Islam, M. T.; Banaszak Holl, M. M. Interaction of polycationic polymers with supported lipid bilayers and cells: nanoscale hole formation and enhanced membrane permeability. *Bioconjugate Chem.* **2006,** 17(3), 728-734.

[42] Lin, Y.; Su, Z. Layer-by-layer assembly of gelatin. *J. Polym. Sci. B Polym. Phys.* **2008,** 46(12), 1252-1257.

[43] Kim, S. W.; Ogawa, T.; Tabata, Y.; Nishimura, I. Efficacy and cytotoxicity of cationic-agent–mediated nonviral gene transfer into osteoblasts. *J. Biomed. Mater. Res. A* **2004**, 71(2), 308-315.

[44] Saito, T.; Tabata, Y. Preparation of gelatin hydrogels incorporating low-molecular-weight heparin for anti-fibrotic therapy. *Acta Biomater.* **2012**, 8(2), 646-652.

[45] Shi, P.; Zhao, N.; Coyne, J.; Wang, Y. DNA-templated synthesis of biomimetic cell wall for nanoencapsulation and protection of mammalian cells. *Nat. Commun.* **2019,** 10(1), 1-11.

[46] Saini, H. K.; Arneja, A. S.; Dhalla, N. S. Role of cholesterol in cardiovascular dysfunction.. *Can. J. Cardiol.* **2004,** 20(3), 333-346.

[47] Sakai, S.; Nomura, K.; Mochizuki, K.; Taya, M. Anchoring PEG-oleate to cell membranes stimulates reactive oxygen species production. *Colloids Surf. B Biointerfaces* **2016,** 147, 336-342.

[48] Vepari, C.; Kaplan, D. L. Silk as a biomaterial, *Prog. Polym. Sci.* **2007,** 32(8-9), 991-1007.

[49] Wang, C., Xia, K., Zhang, Y., & Kaplan, D. L. Silk-Based Advanced Materials for Soft Electronics. *Acc. Chem. Res.* **2019**, 52(10), 2916-2927.

[50] Wang, Q.; Ling, S.; Yao, Q.; Li, Q.; Hu, D.; Dai, Q.; Zhang, Y. Observations of 3 nm silk nanofibrils exfoliated from natural silkworm silk fibers. *ACS Mater. Lett.* **2020**, 2(2), 153-160.

[51] Shao, Z.; Vollrath, F. Surprising strength of silkworm silk. *Nature* **2002,** 418(6899), 741-741.

[52] Jin, H. J.; Kaplan, D. L. Mechanism of silk processing in insects and spiders. *Nature* **2003**, 424(6952), 1057-1061.

[53] Hasturk, O.; Jordan, K. E.; Choi, J.; Kaplan, D. L. Enzymatically crosslinked silk and silk-gelatin hydrogels with tunable gelation kinetics, mechanical properties and bioactivity for cell culture and encapsulation, *Biomaterials* **2020,** 232, 119720.

[54] Murphy, A. R.; Kaplan, D. L. Biomedical applications of chemically-modified silk fibroin. *J. Mater. Chem.* **2009,** 19(36), 6443-6450.

[55] Serban, M. A.; Kaplan, D. L. pH-Sensitive ionomeric particles obtained via chemical conjugation of silk with poly (amino acid)s. *Biomacromolecules* **2010,** 11(12), 3406-3412.

[56] Ye, C.; Drachuk, I.; Calabrese, R.; Dai, H.; Kaplan, D. L.; Tsukruk, V. V. Permeability and micromechanical properties of silk ionomer microcapsules. *Langmuir* **2012,** 28(33), 12235-12244.

[57] Geryak, R.; Quigley, E.; Kim, S.; Korolovych, V. F.; Calabrese, R.; Kaplan, D. L.; Tsukruk, V. V. Tunable Interfacial Properties in Silk Ionomer Microcapsules with Tailored Multilayer Interactions. *Macromol. Biosci.* **2019,** 19(3), 1800176.

[58] Drachuk, I.; Calabrese, R.; Harbaugh, S.; Kelley-Loughnane, N.; Kaplan, D. L.; Stone, M.; Tsukruk, V. V. Silk macromolecules with amino acid–poly (ethylene glycol) grafts for controlling layer-by-layer encapsulation and aggregation of recombinant bacterial cells. *ACS nano* **2015,** 9(2), 1219-1235.

[59] Chu, F. S.; Lau, H. P.; Fan, T. S.; Zhang, G. S. Ethylenediamine modified bovine serum albumin as protein carrier in the production of antibody against mycotoxins. *J. Immunol. Methods* **1982,** 55(1), 73-78.

[60] Mo, X.; Iwata, H.; Matsuda, S.; Ikada, Y. Soft tissue adhesive composed of modified gelatin and polysaccharides. *J. Biomater. Sci. Polym. Ed.* **2000,** 11(4), 341-351.

[61] Sarika, P. R.; James, N. R. Polyelectrolyte complex nanoparticles from cationised gelatin and sodium alginate for curcumin delivery. *Carbohydr. Polym.* **2016,** 148, 354-361.

[62] Hafidz, R.M.R.N.; Yaakob, C.M.; Amin, I.; Noorfaizan, A. Chemical and functional properties of bovine and porcine skin gelatin. *Int. Food Res. J.* **2011,** 18(2011), 813-817.

[63] Murphy, A. R.; John, P. S.; Kaplan, D. L. Modification of silk fibroin using diazonium coupling chemistry and the effects on hMSC proliferation and differentiation. *Biomaterials* **2008,** 29(19), 2829-2838.

[64] Kishore Sahoo, J.K.; Choi, J.; Hasturk, O.; Laubach, I.; Descoteaux, M.L.; Mosurkal, S.; Wang, B.; Zhang, N.; Kaplan, D.L. Silk fibroin degumming time controls horseradish peroxidase-catalyzed hydrogel properties. *Biomater. Sci.* **2020**, paper accepted.

[65] Kuiken, K. A.; Lyman, C. M.; Hale, F.; Dieterich, S.; Bradford, M.; Trant, M. Factors which influence the stability of trytophan during the hydrolysis of proteins in alkaline solution. *J. Biol. Chem.* **1947,** 171, 551-560.

[66] Bruice, T. C.; Fife, T. H.; Bruno, J. J.; Brandon, N. E. Hydroxyl Group Catalysis. II. The Reactivity of the Hydroxyl Group of Serine. The Nucleophilicity of Alcohols and the Ease of Hydrolysis of Their Acetyl Esters as Related to Their pKa. *Biochemistry* **1962,** 1(1), 7-12.

[67] Gulrajani, M. L. Degumming of silk. *Color. Technol.* **1992**, 22(1), 79-89.

[68] Wang, Y. J.; Zhag, Y. Q. Three-layered sericins around the silk fibroin fiber from Bombyx mori cocoon and their amino acid composition. *Adv. Mat. Res.* **2011**, 175,158-163

[69] Shulha, H.; Foo, C. W. P.; Kaplan, D. L.; Tsukruk, V. V. Unfolding the multi-length scale domain structure of silk fibroin protein. *Polymer* **2006**, 47(16), 5821-5830.

[70] Ma, M.; Zhong, J.; Li, W.; Zhou, J.; Yan, Z.; Ding, J.; He, D. Comparison of four synthetic model peptides to understand the role of modular motifs in the self-assembly of silk fibroin. *Soft Matter* **2013**, 9(47), 11325-11333.

[71] Tang, Z.; Johal, M. S.; Scudder, P.; Caculitan, N.; Magyar, R. J.; Tretiak, S.; Wang, H. L. Study of the non-covalent interactions in Langmuir–Blodgett films: An interplay between π− π and dipole–dipole interactions. *Thin Solid Films* **2007**, 516(1), 58-66.

[72] van Vlijmen, H.W.; Schaefer, M.; Karplus, M. Improving the accuracy of protein pKa calculations: conformational averaging versus the average structure. *Proteins* **1998**, 33(2), 145-158.

[73] Saracino, G.A.; Improta, R.; Barone, V. Absolute pKa determination for carboxylic acids using density functional theory and the polarizable continuum model. *Chem. Phys. Lett.* **2003**, 373(3-4), 411-415.

[74] Hollingsworth, C.A.; Seybold, P.G.; Hadad, C.M. Substituent effects on the electronic structure and pKa of benzoic acid. *Int. J. Quantum Chem.* **2002**, 90(4-5), 1396-1403.

[75] Zhou, P.; Xie, X.; Knight, D. P.; Zong, X.H.; Deng, F.; Yao, W.H. Effects of pH and calcium ions on the conformational transitions in silk fibroin using 2D Raman correlation spectroscopy and 13C solid-state NMR. *Biochemistry* **2004**, 43(35), 11302-11311.

[76] Matsumoto, A.; Chen, J.; Collette, A. L.; Kim, U. J.; Altman, G. H.; Cebe, P.; Kaplan, D. L. Mechanisms of silk fibroin sol− gel transitions. *J. Phys. Chem. B*, **2006,** 110(43), 21630-21638.

[77] Heichel, D.; Burke, K. A. Enhancing the Carboxylation Efficiency of Silk Fibroin through the Disruption of Noncovalent Interactions. *Bioconjugate Chem.* **2020**, 31(5), 1307–1312.

[78] Deng, H. Nitrite anions induce nitrosative deamination of peptides and proteins. *Rapid Commun. Mass. Sp.* **2006**, 20(24), 3634-3638.

[79] Collins, C. J. Reactions of primary aliphatic amines with nitrous acid. *Acc. Chem. Res.* **1971**, 4(9), 315-322.

[80] Kaszuba, M.; Corbett, J.; Watson, F. M.; Jones, A. High-concentration zeta potential measurements using light-scattering techniques. *Philos. Trans. R. Soc. A* **2010,** 368(1927), 4439-4451.

[81] Chen, Y.; Yu, B.; Xue, G.; Zhao, J.; Li, R. K.; Liu, Z.; Niu, B. Effects of storage solutions on the viability of human umbilical cord mesenchymal stem cells for transplantation. *Cell Transplant.* **2013,** 22(6), 1075-1086.

[82] Tsui, F. C.; Ojcius, D. M.; Hubbell, W. L. The intrinsic pKa values for phosphatidylserine and phosphatidylethanolamine in phosphatidylcholine host bilayers. *Biophys. J.* **1986**, 49(2), 459.

[83] Narayanan, S. Sialic acid as a tumor marker. *Ann. Clin. Lab. Sci.* **1994**, 24(4), 376-384.

[84] Zhang, Y.; Yang, M.; Portney, N. G.; Cui, D.; Budak, G.; Ozbay, E.; Ozkan, C. S. Zeta potential: a surface electrical characteristic to probe the interaction of nanoparticles with normal and cancer human breast epithelial cells. *Biomed. Microdevices* **2008**, 10(2), 321-328.

[85] Bondar, O. V.; Saifullina, D. V.; Shakhmaeva, I. I.; Mavlyutova, I. I.; Abdullin, T. I. Monitoring of the zeta potential of human cells upon reduction in their viability and interaction with polymers. *Acta Naturae* **2012**, 4(1),78- 81.

[86] Lvov, Y.; Ariga, K.; Onda, M.; Ichinose, I.; Kunitake, T. A careful examination of the adsorption step in the alternate layer-by-layer assembly of linear polyanion and polycation. *Colloids Surf. A Physicochem. Eng. Asp.* **1999,** 146(1-3), 337-346.

[87] Shiratori, S. S.; Yamada, M. Nano-scale control of composite polymer films by mass-controlled layer-by-layer sequential adsorption of polyelectrolytes. *Polym. Adv. Technol.* **2000,** 11(8-12), 810-814.

[88] Steitz, R.; Leiner, V.; Siebrecht, R.; Klitzing, R. V. Influence of the ionic strength on the structure of polyelectrolyte films at the solid/liquid interface. *Colloids Surf. A Physicochem. Eng. Asp.* **2000,** 163(1), 63-70.

[89] Notley, S. M.; Biggs, S.; Craig, V. S.; Wågberg, L. Adsorbed layer structure of a weak polyelectrolyte studied by colloidal probe microscopy and QCM-D as a function of pH and ionic strength. *Phys. Chem. Chem. Phys*. **2004,** 6(9), 2379-2386.

[90] Irigoyen, J.; Han, L.; Llarena, I.; Mao, Z.; Gao, C.; Moya, S. E. Responsive polyelectrolyte multilayers assembled at high ionic strength with an unusual collapse at low ionic strength. *Macromol. Rapid Commun.* **2012,** 33(22), 1964-1969.

[91] Partlow, B. P.; Bagheri, M.; Harden, J. L.; Kaplan, D. L. Tyrosine templating in the self-assembly and crystallization of silk fibroin. *Biomacromolecules* **2016,** 17(11), 3570-3579.

[92] Wang, N.; Zhang, G.; Ji, S.; Qin, Z.; Liu, Z. The salt-, pH-and oxidant-responsive pervaporation behaviors of weak polyelectrolyte multilayer membranes. *J. Membr. Sci.* **2010**, 354(1-2), 14-22.

[93] Mackenzie, C. G.; Mackenzie, J. B.; Beck, P. The effect of pH on growth, protein synthesis, and lipid-rich particles of cultured mammalian cells. *J. Cell Biol.* **1961**, 9(1), 141-156.

[94] Dubas, S. T.; Schlenoff, J. B. Polyelectrolyte multilayers containing a weak polyacid: construction and deconstruction. *Macromolecules* **2001**, 34(11), 3736-3740.

[95] Kovacevic, D.; Van der Burgh, S.; De Keizer, A.; Cohen Stuart, M. A. Kinetics of formation and dissolution of weak polyelectrolyte multilayers: role of salt and free polyions. *Langmuir* **2002**, 18(14), 5607-5612.

[96] Jonker, C. T.; Deo, C.; Zager, P. J.; Tkachuk, A. N.; Weinstein, A. M.; Rodriguez-Boulan, E.; Schreiner, R. Accurate measurement of fast endocytic recycling kinetics in real time. *J. Cell Sci.* **2020**, 133(2), 1-12.

[97] Choi, J.; McGill, M.; Raia, N. R.; Hasturk, O.; Kaplan, D. L. Silk Hydrogels Crosslinked by the Fenton Reaction. *Adv. Healthcare Mater.* **2019**, 8(17), 1900644.

[98] Zhao, H.; Xiong, S.; Li, M.; Zhang, Q.; Liu, G.; Comparison of gelation time and polyalcohol effect on hydrogels from domestic and wild silk fibroins. *Adv. Mater. Sci. Eng*. **2012**, 2012, 1-6.

Table 1. MW of carboxylated and aminated silk constructs extracted by varying degumming times.

Sample		Peak MW (kDa)		Mean MW (kDa)	
Modification	**Degumming time (min)**	**Before amination**	**After amination**	**Before amination**	**After amination**
No Carboxylation (SF)	60	131	123	88	85
	90	98	85	78	99
	120	81	75	70	77
Tyrosine Carboxylated (SF(Y)COOH)	60	108	217	70	84
	90	110	219	70	90
	120	100	226	69	98
Serine Carboxylated (SF(S)COOH)	1	64	70	76	69
	60	36	39	57	66

Table 2. Net charge of the silk constructs estimated by quantification of carboxylic acid and primary amine residues.

	Sample	Net Charge (nmol/mg protein)		Sample	Net Charge (nmol/mg protein)
Carboxylated silk	131 kDa SF	-(143.1 ± 51.2)	**Aminated silk**	123 kDa SF-EDA	+(449.2 ± 31.6)
	98 kDa SF	-(147.0 ± 40.7)		85 kDa SF-EDA	+(429.7 ± 76.5)
	81 kDa SF	-(182.4 ± 54.4)		75 kDa SF-EDA	+(452.7 ± 86.2)
	108 kDa SF(Y)COOH	-(412.3 ± 75.9)		217 kDa SF(Y)-EDA	+(54.3 ± 50.8)
	110 kDa SF(Y)COOH	-(445.9 ± 62.9)		219 kDa SF(Y)-EDA	+(61.7 ± 81.4)
	100 kDa SF(Y)COOH	-(414.2 ± 60.8)		226 kDa SF(Y)-EDA	+(236.7 ± 74.4)
	64 kDa SF(S)COOH	-(261.3 ± 60.3)		70 kDa SF(S)-EDA	+(459.2 ± 74.1)
	36 kDa SF(S)COOH	-(244.5 ± 17.2)		39 kDa SF(S)-EDA	+(493.3 ± 93.3)

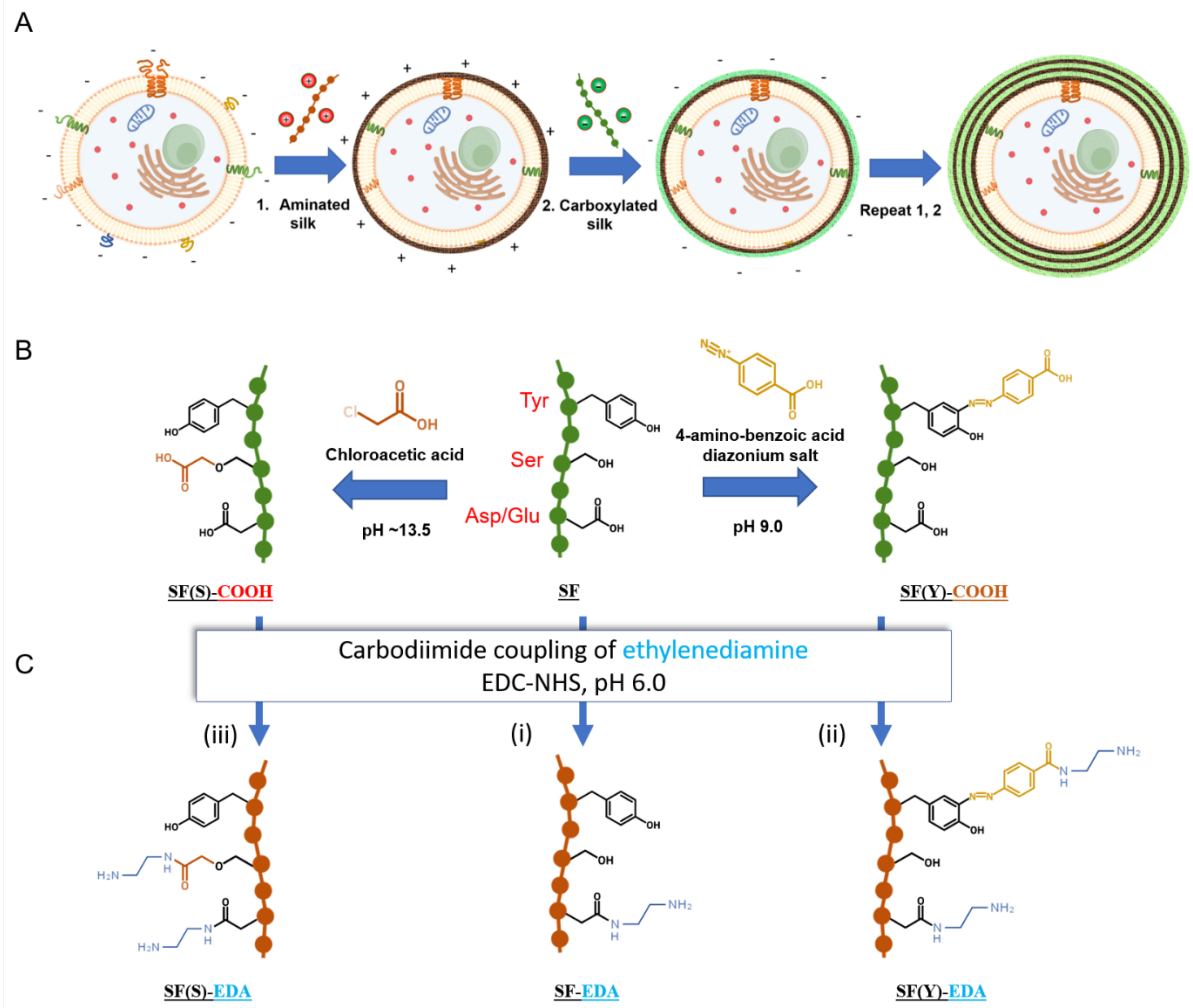

Figure 1. Synthesis and layer-by-layer (LbL) deposition of aminated and carboxylated silks. (A) Schematic showing electrostatic LbL deposition of aminated (+) and carboxylated (-) silk constructs on negatively charged mammalian cell surface. Schematic representation of (B) carboxylation and (C) carbodiimide coupling of ethylenediamine (EDA) residues on (i) unmodified, (ii) tyrosine-carboxylated (SF(Y)COOH) or (iii) serine-carboxylated SF (SF(S)COOH). EDC: 1-Ethyl-3-(3-dimethylaminopropyl) carbodiimide, NHS: N-Hydroxysuccinimide.

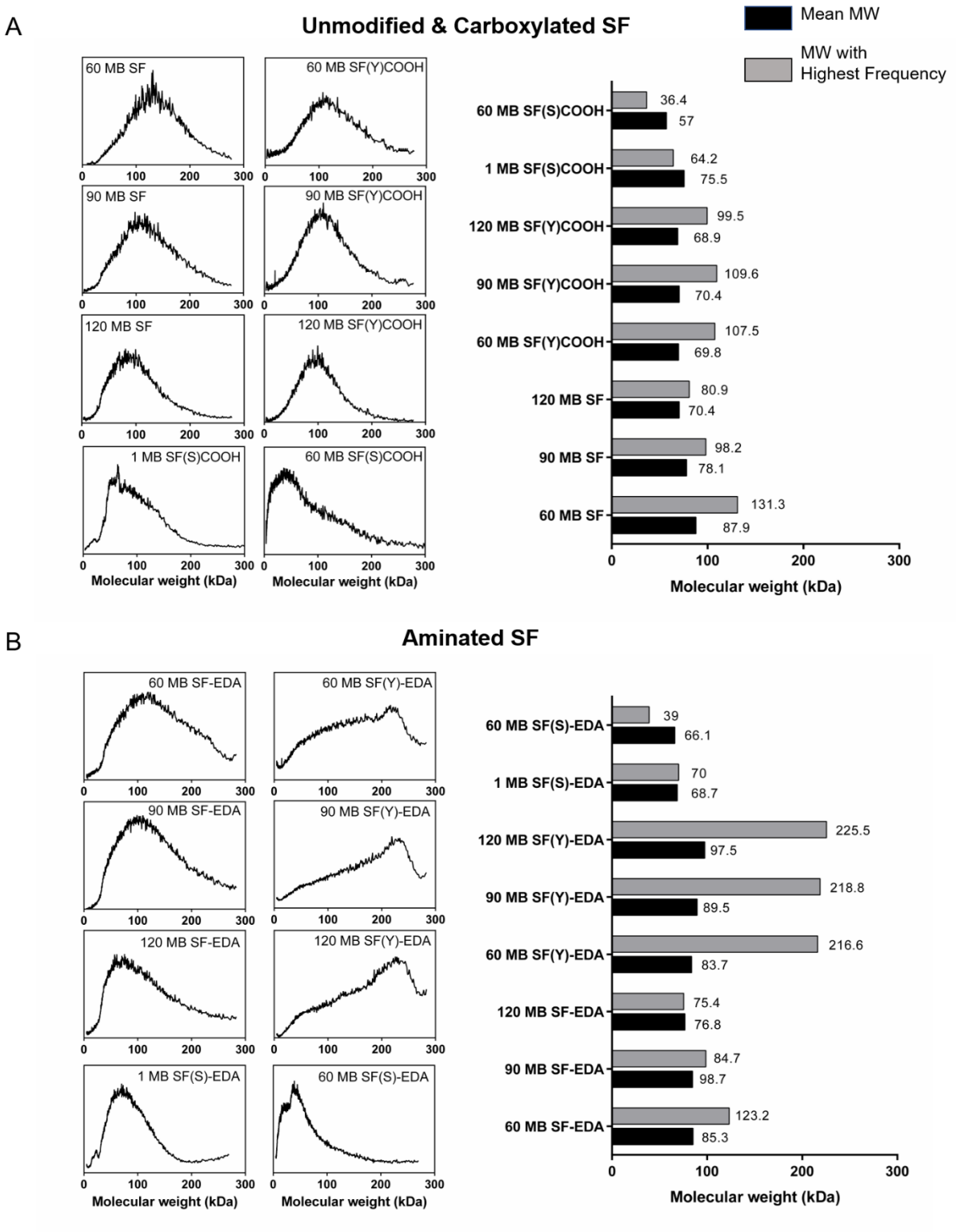

Figure 2. Molecular weight (MW) analysis of (A) unmodified or carboxylated and (B) aminated SF constructs conducted by digital analysis of SDS-PAGE gels. Black bars: mean MW, grey bars: MW with highest frequency.

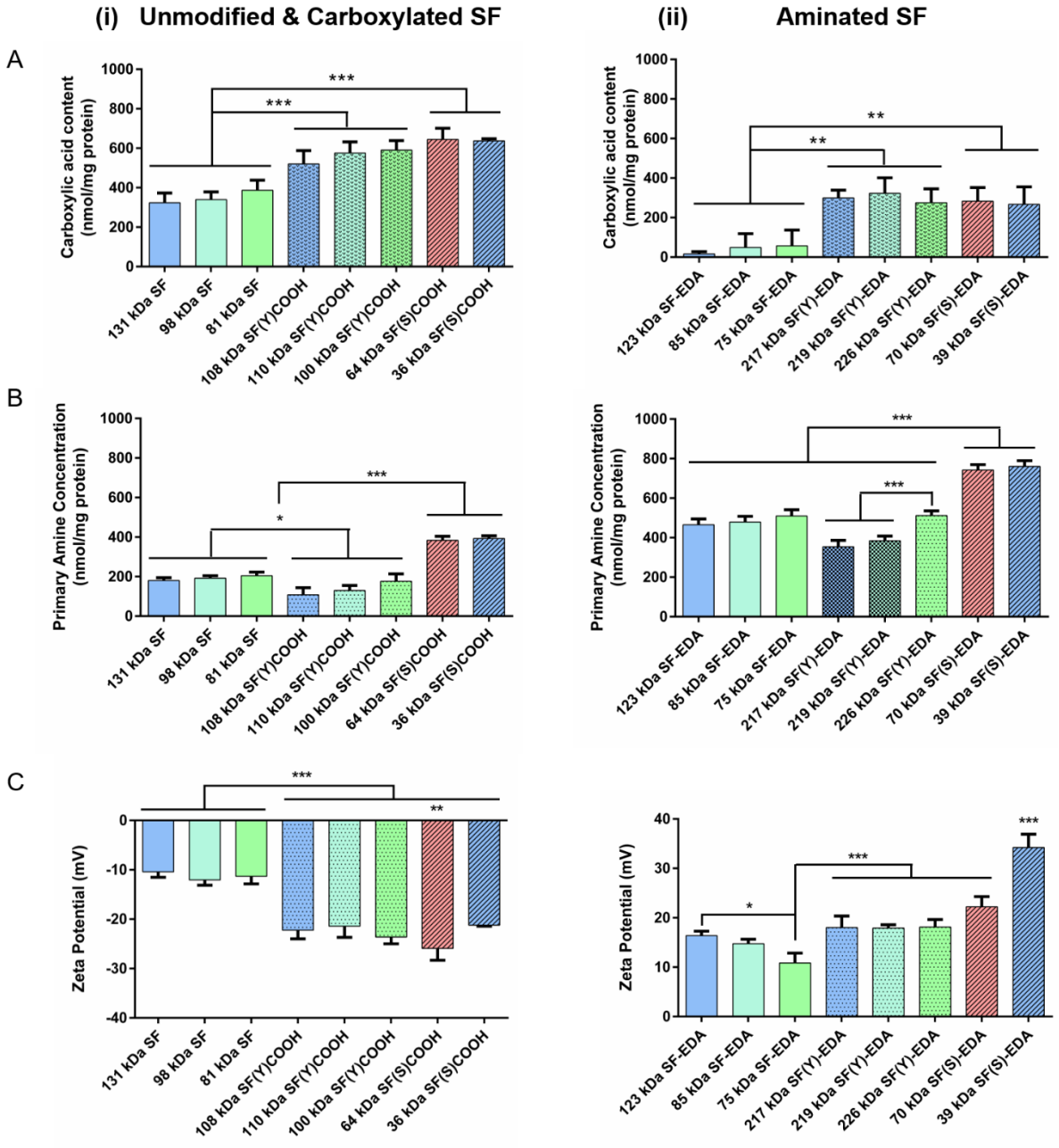

Figure 3. Characterization of the charged residues on silk ionomers. Quantification of the (A) carboxylic acid residues (n=3), (B) primary amine content (n=5) and (C) zeta potential (n=3) of (i) unmodified or carboxylated and (ii) aminated silk constructs. (*$p < 0.05$, **$p < 0.01$ and ***$p < 0.001$).

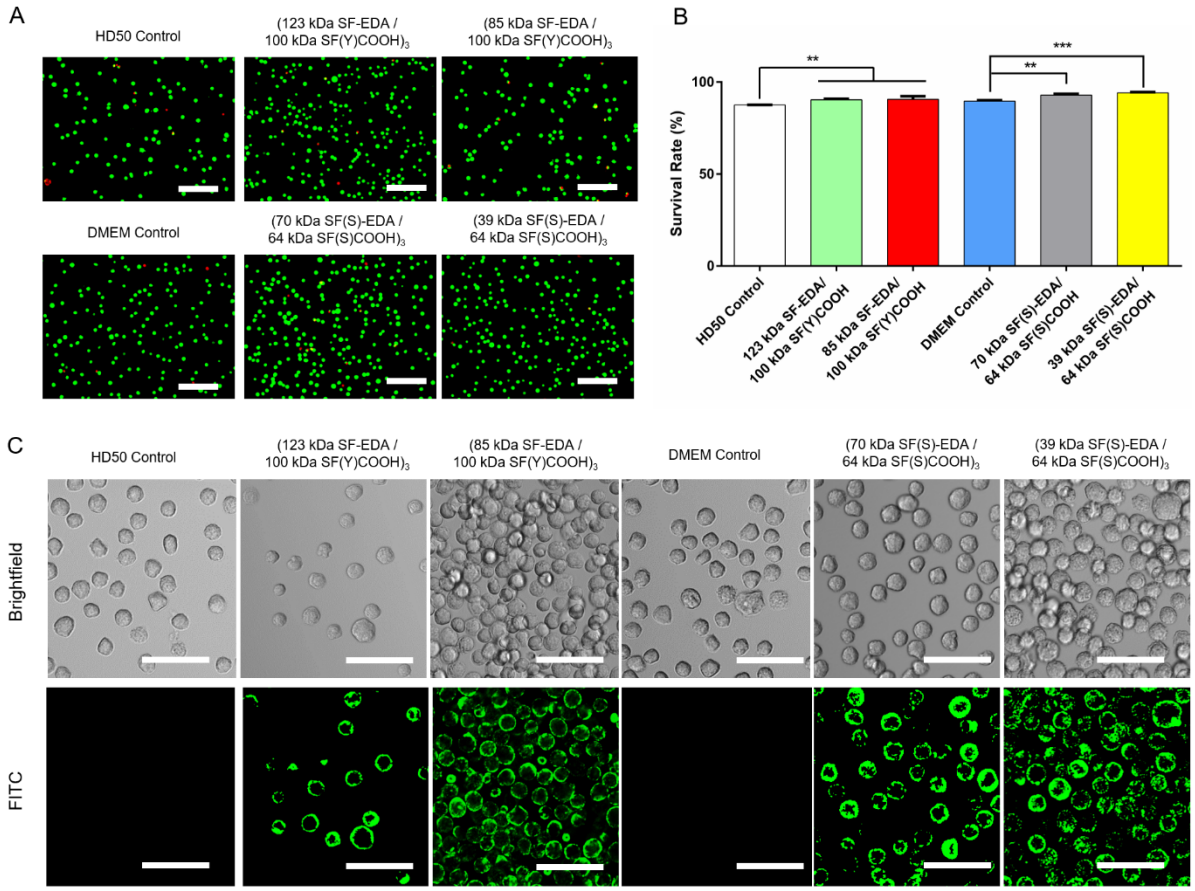

Figure 4. Cytotoxicity and cell surface deposition of 3 silk ionomer bilayers on L929 fibroblasts 2 h after treatment. (A) Fluorescent micrographs of the live/dead stained nanocoated cells. Green: calcein (live), red: EthD-1 (dead), scale bars: 200 µm. (B) Survival rates of the nanocoated cells (n = 3, *p < 0.05, **p < 0.01 and ***p < 0.001). (C) Confocal micrographs of the cells nanocoated with 3 bilayers of FITC-labeled silk ionomers. Scale bars: 50 µm.

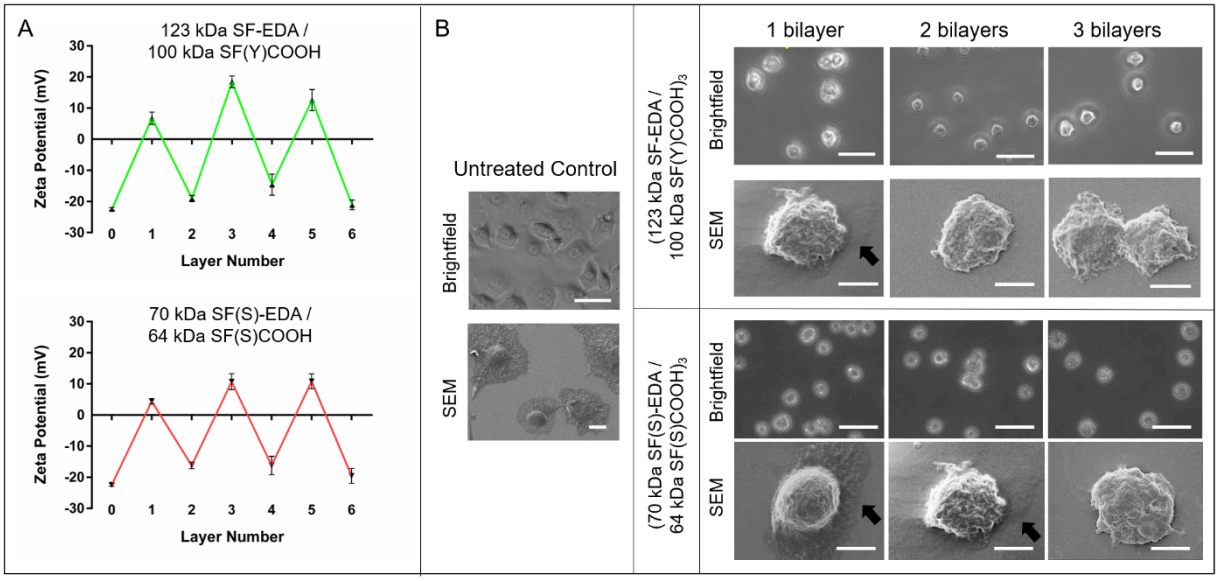

Figure 5. Analysis of the LbL deposition of silk ionomers on L929 cells. (B) Zeta potential measurement of the cells nanocoated with 3 bilayers of silk ionomers (n=3). (B) Brightfield and SEM micrographs of the nanocoated cells taken 10 h after treatment. Black arrows on SEM micrographs point out lamellipodia layers beneath the cells. Scale bars; brightfield: 50 µm, SEM: 5 µm.

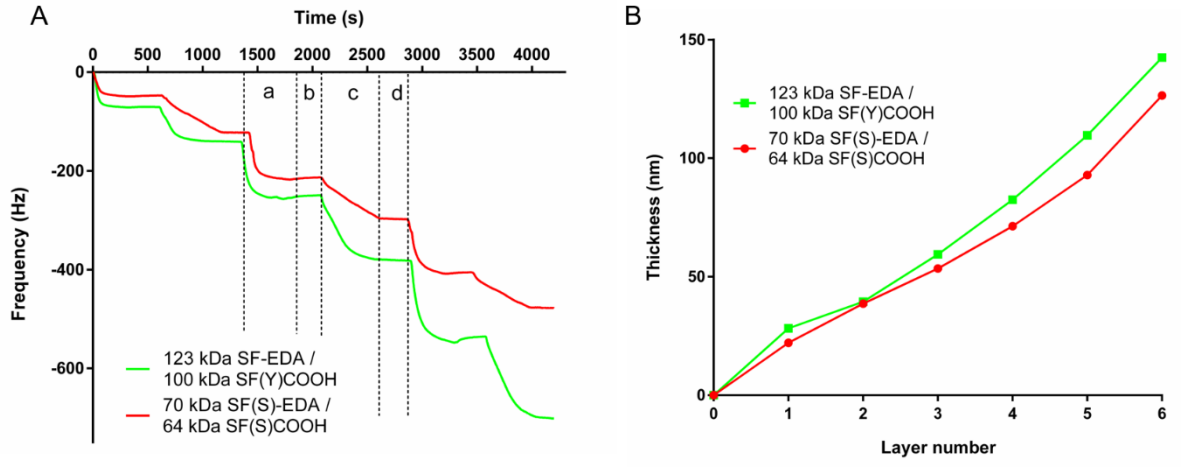

Figure 6. QCM-D analysis of LbL deposition of positively and negatively charged silk ionomer pairs. (A) The change in the composite resonance frequency of oscillating quartz crystal with increasing number of ionomer layers deposited on the sensor. **Step a**: deposition of aminated (+) silk, **b:** rinsing, **c:** deposition of carboxylated (-) silk, **d:** rinsing. (B) Thickness of the ionomer multilayers estimated by viscoelastic model.

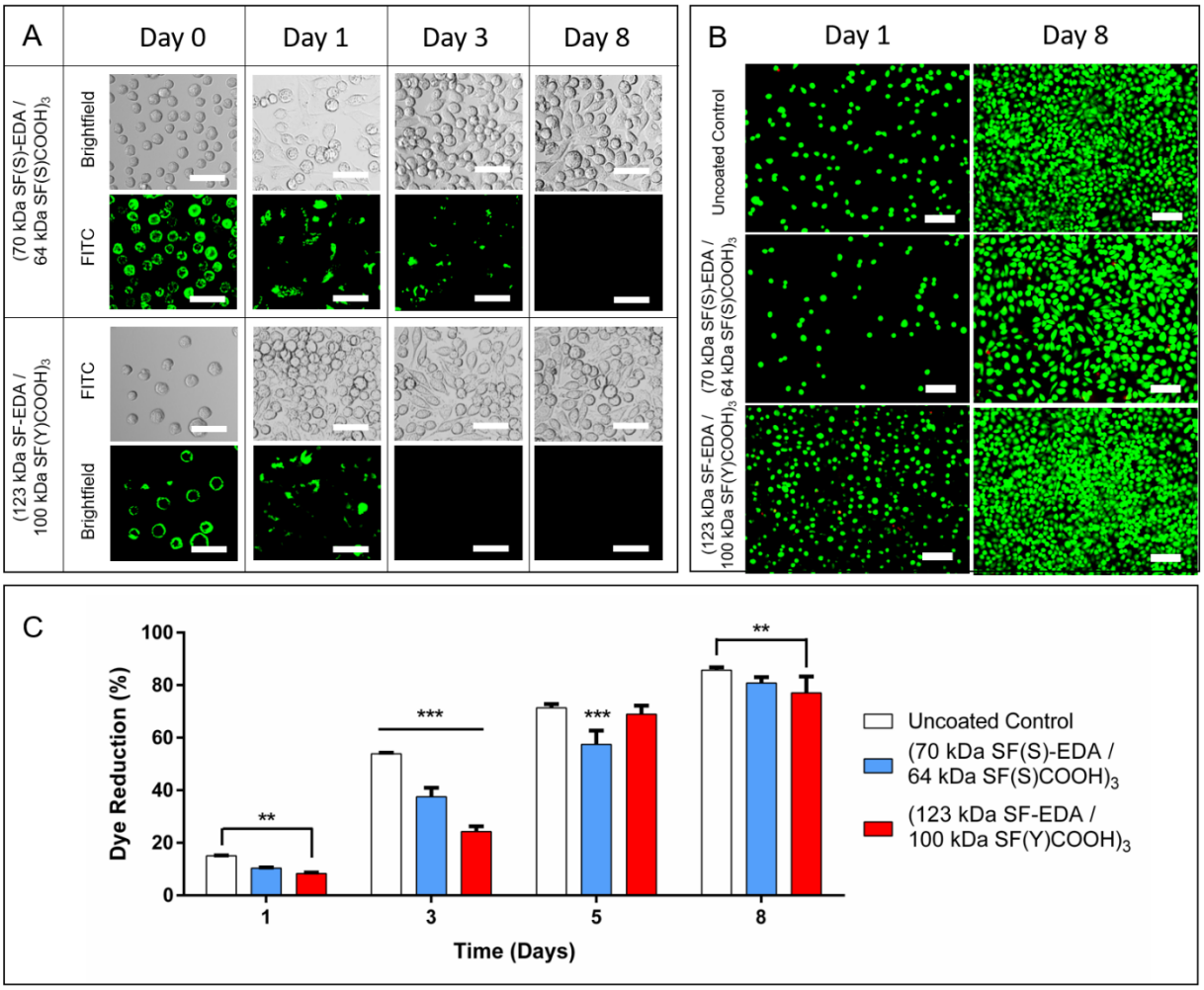

Figure 7. Analysis of nanocoated L929 fibroblasts over 8 days of culture. (A) Confocal micrographs of the cells. Green: FITC-labeled silk ionomers, scale bars: 50 µm. (B) Fluorescent micrographs of the live/dead stained cells at days 1 and 8. Green: calcein (live), red: EthD-1 (dead), scale bars: 200 µm. (C) % dye reduction by the nanocoated cells depicting metabolic activity (n = 4, *p < 0.05, **p < 0.01 and ***p < 0.001).

For Table of Contents Only